Eur. Phys. J. B **51**, 101–110 (2006)
DOI: 10.1140/epjb/e2006-00195-8

THE EUROPEAN PHYSICAL JOURNAL B

Phase diagrams of Ising fluids with Yukawa-Lennard-Jones interactions from an integral equation approach

I.P. Omelyan[1,2], W. Fenz[2,a], R. Folk[2], and I.M. Mryglod[1,2]

[1] Institute for Condensed Matter Physics, 1 Svientsitskii Street, UA-79011 Lviv, Ukraine
[2] Institute for Theoretical Physics, Linz University, A-4040 Linz, Austria

Received 21 December 2005 / Received in final form 7 March 2006
Published online 31 May 2006 –

Abstract. An integral equation approach is developed to investigate phase coexistence properties of Ising spin fluids with Yukawa ferromagnetic and Lennard-Jones nonmagnetic interactions in the presence of an external field. The calculations are carried out on the basis of the Duh and Henderson closure with a specific Duh-like partitioning of the total potential. The coupled set of the Ornstein-Zernike equation, the closure relation and the external field constraint are solved using an efficient numerical algorithm. The phase diagrams are evaluated in a wide range of varying the external field and the ratio of strengths of Yukawa to Lennard-Jones interactions. Different types of the phase diagram topology as well as various external field dependencies of critical temperatures and densities are identified. The complexity with respect to simple Lennard-Jones fluids is explained by coupling between spatial and spin degrees of freedom in the system. A comparison of the obtained theoretical results with simulation data is made and a good agreement is observed.

PACS. 64.60.-i General studies of phase transitions – 64.70.Fx Liquid-vapor transitions – 75.50.Mm Magnetic liquids

1 Introduction

Fluids with ferromagnetic spin interactions have been intensively studied during the past several decades [1–25]. Mean field (MF) approaches [1,2,4,12,13,18–20,25], integral equation (IE) theories [3,9–11,14–16,21–24], as well as Monte Carlo (MC) simulation techniques [3,5–8,11,17–25] have been used to investigate thermodynamic, magnetic, and critical properties of spin fluids. Various spin fluid models, such as the Ising, XY and Heisenberg ones, with different types of magnetic and nonmagnetic interactions have been considered. As was established, these models exhibit a rich variety in the phase diagram behaviour. It is characterized by the existence of critical, tricritical, critical end, and triple points related to phase transitions between gas, liquid, paramagnetic and ferromagnetic states. Similar phase diagrams have been found in other systems including spin lattice gas models [26,27], binary mixtures [28–38], He^3-He^4 mixtures [39–41], etc.

Previous IE studies of spin fluids have been restricted mainly to so-called ideal models, where the attractive nonmagnetic interactions are absent [3,9–11,14,16,24]. More complicated nonideal models have also been considered [15,21–23]. However, both magnetic and attractive nonmagnetic potentials were assumed to be of the same Yukawa-type (YK) form (such models will be referred to as YK-YK). While the exchange integral of spin interactions can indeed be expressed in terms of the YK function, it is generally believed that in real systems the attraction part of nonmagnetic interactions at long distances has the asymptotic form of the Lennard-Jones (LJ) potential. Despite this, the development of an IE approach for spin fluids with LJ nonmagnetic interactions has never been addressed.

In the IE consideration of YK-YK models, the repulsion part of nonmagnetic interactions was modeled either by the hard-sphere potential [3,9–11,14–16] or a soft-core function [21–23]. The latter can be obtained by shifting and truncating the LJ function at short distances of order of the size of the interacting particles [20,21]. This of course has nothing to do with the original LJ potential which includes both the soft-core repulsion as well as the long-range attraction in the form of the inverse (12-6) power law dependence on interparticle separation. This is contrary to the case of the YK potential where the interaction decays exponentially with increasing the distance between interacting particles.

Until now, only one work [19] dealt with the more natural case of LJ nonmagnetic and YK magnetic interactions (the corresponding model will be referred to as LJ-YK). The calculations in this work have been performed for the LJ-YK Ising model in the absence of an external field using

[a] e-mail: wolfgang.fenz@jku.at

MC simulation techniques as well as a van der Waals-like version of the MF theory. However, no explicit relations connecting the parameters of the van der Waals equation of state with the microscopic parameters of the LJ and YK potentials have been in fact presented. Moreover, the MF approximation can give only qualitative results, since it neglects pair correlations in spin space [20–23]. A more precise IE consideration is required to obtain a quantitative description. Besides the theoretical interest, this may be important from a practical point of view as well, because the Ising model can be applied to the description of phase transitions in real systems such as inert fluids, Au-Co and $Co_{80}Pd_{20}$ melts [42,43], etc.

The existing IE approaches for spin fluids with YK interactions are based exclusively on the (hard or soft) mean spherical approximation (MSA) for the bridge function [21–23]. The MSA has proved to be very accurate when handling the YK magnetic and nonmagnetic correlations in the Ising [21] and XY [22,23] spin fluids. However, this approximation is not necessarily as good for other types of interactions. The most notorious example is the pure LJ fluid, where the soft MSA (SMSA) combined with the standard Weeks, Chandler, and Andersen (WCA) partitioning scheme [44] does not provide a quantitative description and more precise approximations of the bridge function are needed [45]. Among them it is worth mentioning the reference hypernetted chain (RHNC) approximation [45,46], a modification of the original hypernetted chain (HNC) approach, the HNC-MSA (HMSA) [47–49], as well as the Duh and Henderson (DH) closure which includes a specific partitioning of the LJ potential [45,50, 51].

The RHNC requires minimization of the free energy and its extension to spin fluids leads to tremendous computational efforts. Similar difficulties arise with an extension of the HMSA, because it also demands time-consuming evaluations of the Helmholtz free energy (an explicit expression for which appears to be too complicated when involving spin degrees of freedom). On the other hand, the DH closure is simpler in the implementation and provides nearly the same level of accuracy as the cumbersome RHNC and HMSA schemes. Quite recently, it has been shown that the DH partitioning can also be successfully used in an inhomogeneous IE description of the LJ fluid, leading to a quantitative evaluation of density profiles at the gas-liquid interface [52].

In this paper we propose an extension of the DH approach to fluid systems with both translational and spin interactions. It consists in a modification of the DH closure to the Ornstein-Zernike (OZ) equation in the presence of an external field constraint by using a specific Duh-like partitioning of the full potential. The theory is applied to the LJ-YK Ising spin fluid model and the obtained phase diagrams are compared with simulation data. The dependencies of critical temperatures and densities on the external field are analyzed as well. The paper is organized as follows. The theory is described in Section 2. The results are presented and discussed in Section 3. Concluding comments are given in Section 4.

2 Theory

2.1 Model

Let us consider a system of point particles with embedded Ising spins described by the Hamiltonian

$$H = \sum_{i<j}^{N} \Big[\varphi(r_{ij}) - J(r_{ij})\, s_i s_j\Big] - B\sum_{i=1}^{N} s_i\,. \tag{1}$$

Here, N is the total number of particles, $\varphi(r)$ and $J(r)$ denote the potential and exchange integral correspondingly of nonmagnetic and spin-spin interactions, $\mathbf{r}_i$ designates the three dimensional (3D) spatial coordinate of the ith particle carrying spin s_i, B relates to the external magnetic field, and $r_{ij} = |\mathbf{r}_i - \mathbf{r}_j|$ is the interparticle separation. In the LJ-YK Ising spin fluid model, the nonmagnetic potential is chosen in the form of the 12-6 LJ function

$$\varphi(r) = 4\varepsilon\left[\left(\frac{\sigma}{r}\right)^{12} - \left(\frac{\sigma}{r}\right)^{6}\right], \tag{2}$$

while the spin interactions are described by the YK exchange integral

$$J(r) = \frac{\epsilon\sigma}{r}\exp\left[-\frac{r-\sigma}{\sigma}\right], \tag{3}$$

where ε and ϵ are the intensities of nonmagnetic and magnetic interactions, respectively, and σ denotes the size of the particles.

The Ising spins take only two values, i.e. $s_i = \pm 1$, $i = 1, 2, \ldots, N$. Thus, the system can be mapped onto a binary mixture with N^+ and N^- particles of type "+" (spin up) and "−" (spin down), respectively, where $N^+ + N^- = N$. Then equation (1) reduces to

$$H = \sum_{i<j}^{N^+}\phi_{++}(r_{ij}) + \sum_{i<j}^{N^-}\phi_{--}(r_{ij}) + \sum_{i,j=1}^{N^+,N^-}\phi_{+-}(r_{ij}) - BM, \tag{4}$$

where $M = \sum_{i=1}^{N} s_i = N^+ - N^-$ relates to the magnetization of the system and

$$\begin{aligned}\phi_{++}(r) &= \phi_{--}(r) = \varphi(r) - J(r)\,,\\ \phi_{+-}(r) &= \phi_{-+}(r) = \varphi(r) + J(r)\end{aligned} \tag{5}$$

are the potentials of interactions between like and unlike particles, respectively.

2.2 Integral equations

According to the liquid state theory [53,54], a complete description of the system can be carried out in terms of the total and direct correlation functions $h_{\alpha\beta}$ and $c_{\alpha\beta}$. Such functions satisfy the OZ equation which for the mixture takes the form

$$h_{\alpha\beta}(r) = c_{\alpha\beta}(r) + \sum_{\gamma=+,-}\rho_\gamma\int c_{\alpha\gamma}(|\mathbf{r}-\mathbf{r}'|)\, h_{\gamma\beta}(r')\,\mathrm{d}\mathbf{r}'\,, \tag{6}$$

where $\rho_\pm = N^\pm/V$ are the partial number densities with V being the volume of the system, and indexes α, β, γ accept two values "+" and "−".

Further, a closure relation must be defined. Its general form is

$$h_{\alpha\beta}(r) = \exp\Big[-\frac{\phi_{\alpha\beta}(r)}{k_{\rm B}T} + h_{\alpha\beta}(r) - c_{\alpha\beta}(r) + b_{\alpha\beta}(r)\Big] - 1\,, \quad (7)$$

where $b_{\alpha\beta}$ denotes the bridge function and $k_{\rm B}T$ is the temperature with the Boltzmann constant. The bridge function cannot be determined exactly within any theory, but there are many approaches enabling to approximate it. The crudest among them is the HNC approximation which corresponds simply to putting $b \equiv 0$. More accurate approximations, such as the RHNC, HMSA, SMSA, and DH [46,48–51,53] lead, as was mentioned in the introduction, to more sophisticated calculations. It has been shown for the pure LJ fluid and its mixtures that an efficient description follows from the DH approximation [38,45,50, 51]. The DH bridge function reads

$$b_{\alpha\beta}(r) = -\frac{s_{\alpha\beta}^2}{2}\,\frac{1}{1 + s_{\alpha\beta}(5s_{\alpha\beta}+11)/(7s_{\alpha\beta}+9)} \quad (8)$$

for $s_{\alpha\beta} > 0$ and $b_{\alpha\beta}(r) = -s_{\alpha\beta}^2/2$ at $s_{\alpha\beta} \le 0$ with $s_{\alpha\beta}(r)$ being the renormalized indirect correlation function.

In our case, according to equation (5), the indirect correlation function can be cast in the form

$$s_{\alpha\beta}(r) = h_{\alpha\beta}(r) - c_{\alpha\beta}(r) - \frac{\varphi_{\rm lr}(r) \mp J_{\rm lr}(r)}{k_{\rm B}T}\,, \quad (9)$$

where $\varphi_{\rm lr}(r)$ and $J_{\rm lr}(r)$ are the long-ranged parts of the LJ and YK potentials, respectively. Like for pure LJ fluids, we choose the DH partitioning [51] for the nonmagnetic part of the potential,

$$\varphi_{\rm lr}(r) = -4\varepsilon\left(\frac{\sigma}{r}\right)^6 \exp\left[-\frac{1}{\rho^*}\left(\frac{\sigma}{r}\right)^{6\rho^*}\right], \quad (10)$$

where $\rho^* = \rho\sigma^3 = (N/V)\sigma^3$ is the dimensionless density. On the other hand, like for ideal Ising fluids with YK magnetic interactions it is quite natural to choose the long-ranged part of $J(r)$ in the Boltzmann-like form [21],

$$J_{\rm lr}(r) = J(r)\exp\left[-\frac{\varphi_{\rm s}(r)}{k_{\rm B}T}\right], \quad (11)$$

where $\varphi_{\rm s}(r)$ denotes the repulsion part of the shifted LJ-potential, i.e., $\varphi_{\rm s}(r) = \varphi(r) + \varepsilon$ at $r < \sqrt[6]{2}\sigma$ and $\varphi_{\rm s}(r) = 0$ for $r \ge \sqrt[6]{2}\sigma$. In the limiting case $\epsilon \to 0$ of the absence of magnetic interactions we obtain the original DH closure.

2.3 External field constraint

From thermodynamic relations it follows that the Gibbs free energy of a nonmagnetic binary mixture has the form

$$G = \mu_+ N^+ + \mu_- N^-\,, \quad (12)$$

where μ_+ and μ_- are the chemical potentials of species "+" and "−", respectively. At the same time, the Gibbs free energy of a magnetic fluid in the presence of an external field is

$$G = \mu N - BM\,. \quad (13)$$

Taking into account the equalities $N = N^+ + N^-$ and $M = N^+ - N^-$, one obtains that both forms of G are identical if and only if

$$B = \frac{\mu_- - \mu_+}{2}\,, \quad (14)$$

$$\mu = \frac{\mu_+ + \mu_-}{2}\,. \quad (15)$$

The latter quantity (Eq. (15)) should be related to the chemical potential of the Ising fluid. Equation (14) forms the so-called external field constraint (FC) which should be imposed on the chemical potentials of the two species to perform an equivalent mapping from the binary mixture description to the Ising fluid representation [21].

It is worth mentioning that when flipping all N^+ spins from up ($s = +1$) to down ($s = -1$) and all N^- spins from down to up (then, in particular, $N^+ \leftrightarrow N^-$) without changing their spatial coordinates, the sum of the first three terms on the right-hand side of equation (4) remains unchanged. This is so due to the symmetrical properties of the binary potentials (see Eq. (5)). During such a mutual exchange the change in the magnetization is $\Delta M = -2(N^+ - N^-) = -2M$ and we have that $\Delta H = -B\Delta M = 2BM$. On the other hand, the corresponding change in the Gibbs free energy according to equations (12) and (14) is equal to $\Delta G = (\mu_- - \mu_+)(N^+ - N^-) = 2BM$ (the same result follows from Eq. (13), since μ and N are invariant with respect to the above transformation $N^+ \leftrightarrow N^-$). Therefore, $\Delta G = \Delta H = 2BM$.

The independent variables in the binary mixture description are the total density ρ and concentration x, i.e.,

$$\rho = \rho_+ + \rho_- = \frac{N}{V}\,, \quad x = \frac{N_+}{N}\,, \quad 1 - x = \frac{N_-}{N}\,. \quad (16)$$

Thus $\mu_\pm = \mu_\pm(\rho, x, T)$ and equation (14) can be presented in a more explicit form,

$$\mu_-(\rho, x, T) - \mu_+(\rho, x, T) = 2B\,. \quad (17)$$

In the Ising fluid representation, at any given values ρ, T, and B, the external field constraint (Eq. (17)) should be solved,

$$x = x(\rho, T, B)\,, \quad (18)$$

and the mapping from (ρ, x, T) to the new set $\big(\rho, x(\rho, T, B), T\big) \equiv (\rho, T, B)$ of variables should be performed [21]. Since $M = N^+ - N^- = xN - (1-x)N = (2x-1)N$, the solution (18) is related to the magnetization per particle

$$m = \frac{M}{N} = 2x - 1 \equiv m(\rho, T, B) \quad (19)$$

of the Ising fluid.

2.4 Thermodynamic and magnetic quantities

Using standard formulas [53,54] for binary mixtures one finds that the pressure can be calculated from the virial equation of state

$$P(\rho,x,T)=\rho k_{\mathrm{B}}T-\frac{2\pi}{3}\sum_{\alpha,\beta}^{+,-}\rho_\alpha\rho_\beta\int_0^\infty\frac{\mathrm{d}\phi_{\alpha\beta}}{\mathrm{d}r}g_{\alpha\beta}(r)r^3\mathrm{d}r\,, \tag{20}$$

where $\rho_+=x\rho$, $\rho_-=(1-x)\rho$, and $g_{\alpha\beta}(r)=h_{\alpha\beta}(r)+1$ denotes the radial distribution function. The chemical potentials can be evaluated using the Kirkwood formula as [21,45,55]

$$\begin{aligned}\mu_\alpha(\rho,x,T)&=k_{\mathrm{B}}T(\ln\rho_\alpha+3\ln\Lambda_\alpha)+k_{\mathrm{B}}T\sum_{\beta=+,-}\rho_\beta\\&\times\int_0^\infty\Big[\frac{1}{2}h_{\alpha\beta}^2(r)-\frac{1}{2}h_{\alpha\beta}(r)c_{\alpha\beta}(r)-c_{\alpha\beta}(r)\\&+b_{\alpha\beta}(r)g_{\alpha\beta}(r)-\frac{h_{\alpha\beta}(r)}{s_{\alpha\beta}(r)}\int_0^{s_{\alpha\beta}(r)}b_{\alpha\beta}(s')\mathrm{d}s'\Big]4\pi r^2\mathrm{d}r\,,\end{aligned} \tag{21}$$

where Λ_α denotes the de Broglie thermal wavelength. Taking into account equation (8), the integration in equation (21) with the DH bridge function can be carried out analytically,

$$\begin{aligned}\int_0^{s_{\alpha\beta}(r)}b_{\alpha\beta}(s')\mathrm{d}s'&=\frac{1}{500}\Big\{5s_{\alpha\beta}(r)\big[162-35s_{\alpha\beta}(r)\big]\\&+2250\ln\frac{3}{3+s_{\alpha\beta}(r)}+36\ln\frac{3}{3+5s_{\alpha\beta}(r)}\Big\}\end{aligned} \tag{22}$$

for $s_{\alpha\beta}(r)>0$ and $\int_0^{s_{\alpha\beta}(r)}b(s')\mathrm{d}s'=-s_{\alpha\beta}^3(r)/6$ for $s_{\alpha\beta}(r)\le 0$.

In view of the explicit expressions (Eqs. (21) and (22)) for the chemical potentials $\mu_\pm$ and the corresponding solution (Eq. (18)) to the external FC (Eq. (17)), the pressure of the Ising fluid can be evaluated according to equation (20) as $P(\rho,x,T)=P(\rho,x(\rho,T,B),T)\equiv P(\rho,T,B)$. Similarly all other thermodynamic and magnetic quantities of the Ising fluid system can be calculated. In particular, the magnetic susceptibility can be obtained by differentiating equation (19) at constant values of ρ and T as $\chi=\rho\,\partial m(\rho,T,B)/\partial B$.

2.5 Phase separations

The phase transitions between gas and liquid states can be determined at a given temperature T from the mechanical and chemical equilibrium conditions

$$\begin{aligned}P\big(\rho^{\mathrm{I}},x^{\mathrm{I}},T\big)&=P\big(\rho^{\mathrm{II}},x^{\mathrm{II}},T\big)\,,\\\mu_+\big(\rho^{\mathrm{I}},x^{\mathrm{I}},T\big)&=\mu_+\big(\rho^{\mathrm{II}},x^{\mathrm{II}},T\big)\equiv\mu_+^{\mathrm{I,II}}\,,\\\mu_-\big(\rho^{\mathrm{I}},x^{\mathrm{I}},T\big)&=\mu_-\big(\rho^{\mathrm{II}},x^{\mathrm{II}},T\big)\equiv\mu_-^{\mathrm{I,II}}\,,\end{aligned} \tag{23}$$

where $\rho^{\mathrm{I,II}}$ and $x^{\mathrm{I,II}}$ are the densities and concentrations of coexisting phases I and II. The conditions should be complimented by the external FC (Eq. (17)) which now reads

$$\mu_-^{\mathrm{I,II}}-\mu_+^{\mathrm{I,II}}=2B\,. \tag{24}$$

In view of the solution $x=x(\rho,T,B)$ (see Eq. (18)) which automatically satisfies equation (24), the coexistence conditions (Eq. (23)) reduce to the form

$$\begin{aligned}P\big(\rho^{\mathrm{I}},T,B\big)&=P\big(\rho^{\mathrm{II}},T,B\big)\,,\\\mu\big(\rho^{\mathrm{I}},T,B\big)&=\mu\big(\rho^{\mathrm{II}},T,B\big)\,,\end{aligned} \tag{25}$$

where $\mu(\rho,T,B)\equiv\mu(\rho,x(\rho,T,B),T)$ is the chemical potential of the Ising fluid (Eq. (15)). This form is similar to that of a simple fluid, but the additional dependence of P and μ on the external field B should be taken into account.

The paramagnetic-ferromagnetic transition in the Ising fluid can be found as a boundary Curie curve $T_\lambda(\rho)$ in the temperature-density plane below which, i.e., for $T<T_\lambda(\rho)$, nonzero (spontaneous) magnetization $m\neq 0$ (see Eq. (19)) becomes possible in the absence ($B=0$) of an external field. On the other hand, for $T>T_\lambda(\rho)$, only the trivial solution $m=0$ will be obtained at $B=0$.

3 Results

3.1 Numerical and simulation details

The coupled set of OZ-DH-FC integro-algebraic equations (6), (7), and (17) together with complementary relations (8)–(11) and (21) was iteratively solved with respect to functions $h_{\alpha\beta}$ and $c_{\alpha\beta}$ by adapting the MDIIS (modified direct inversion in the iterative subspace) algorithm [21–24,56]. The OZ equations (Eq. (6)) were first reduced to the linear system $h_{\alpha\beta}(k)=c_{\alpha\beta}(k)+\sum_{\gamma=+,-}\rho_\gamma c_{\alpha\gamma}(k)\,h_{\gamma\beta}(k)$ by applying the Fourier transform $A(k)=\int_V A(r)\exp(\mathrm{i}\mathbf{k}\cdot\mathbf{r})\mathrm{d}\mathbf{r}=\int_0^{r_{\max}}4\pi r^2A(r)\sin(kr)/(kr)\mathrm{d}r$ within a finite but sufficiently large r-domain of size $r_{\max}\gg\sigma$. The OZ equations were further solved analytically in k-space as $\mathbf{h}(k)=[\mathbf{I}-\mathbf{c}(k)\boldsymbol{\rho}]^{-1}\mathbf{c}(k)$, where $\mathbf{h}$ and $\mathbf{c}$ are the matrices with elements $h_{\alpha\beta}(k)$ and $c_{\alpha\beta}(k)$, respectively, $\boldsymbol{\rho}=\mathrm{diag}(\rho_+,\rho_-)$ is a diagonal matrix and $\mathbf{I}$ denotes the unit matrix. Then applying the backward Fourier transform, the residuals to the DH closure (Eq. (7)) and FC relation (Eq. (17)) have been calculated and the MDIIS procedure was repeated until the solutions $h_{\alpha\beta}(r)$ and $c_{\alpha\beta}(r)$ have converged with a relative root mean square residual uncertainty of 10^{-6}.

The ratio R of strengths of YK ferromagnetic ($\epsilon\ge 0$) to LJ nonmagnetic ($\varepsilon>0$) interactions was introduced as

$$R=\frac{\epsilon}{\varepsilon}\ge 0\,. \tag{26}$$

In the presentation, we use the dimensionless density $\rho^*=\rho\sigma^3$, temperature $T^*=k_{\mathrm{B}}T/\varepsilon$, and external field $B^*=B/\varepsilon$.

The simulations were carried out using the Gibbs ensemble MC (GEMC) approach [57] and the grand canonical ensemble MC method combined with multiple histogram reweighting (MHR) techniques [58] for evaluating the gas-liquid and liquid-liquid transitions. The Binder crossing scheme [17,59] based on canonical MC was employed to determine the paramagnetic-ferromagnetic transition (at $B = 0$). Other simulation details are similar to those reported in references [17,19–21]. Some simulation data for $B = 0$ have been taken from reference [19].

3.2 Zero magnetic field

3.2.1 IE versions

The results for gas-liquid and liquid-liquid coexistence densities of the LJ-YK Ising fluid obtained within the OZ-DH-FC approach in the absence ($B = 0$) of an external field for different ratios $R = 0, 0.05, 0.075, 0.09, 0.1, 0.115, 0.1333$, and 0.2 are presented in Figure 1 by the short-dashed curves. The magnetic transition is shown by the thin lines. The coexistence densities were evaluated using explicitly the equilibrium conditions (Eq. (25)). This evaluation scheme we will refer to as the explicit equating of the pressure and chemical potential (EPCP). The EPCP evaluation has been carried out at $r_{\max} = 10\sigma \gg \sigma$. Further increasing $r_{\max}$ does not affect the solutions. The corresponding GEMC and MHR data are plotted in Figure 1 by open and full circles, respectively. As can be seen, the theoretical and simulation predictions agree well except in the critical regions, where the EPCP, GEMC and MHR binodals terminate.

The termination is explained by the appearance of huge density fluctuations which cannot be properly handled neither by the GEMC and MHR techniques because of the finiteness of the simulation boxes nor by the OZ-DH-FC theory due to the approximate character of the DH closure. Within the OZ-DH-FC approach the termination means that the desired solutions $\rho^{\mathrm{I,II}}$ to the set of EPCP equations (Eq. (25)) begin to disappear when approaching critical temperatures too close. Note that the chemical potential μ (Eq. (15)) evaluated directly in terms of correlation functions (Eq. (21)) is not (to some extent) thermodynamically self-consistent with the pressure P obtained via the virial route (Eq. (20)), because the correlation functions themselves are calculated only approximately. In particular, the Gibbs-Duhem thermodynamic relation $\rho(\partial\mu/\partial\rho)_{T,B} = (\partial P/\partial\rho)_{T,B}$ (connecting the pressure and chemical potential) will not be satisfied exactly. This discrepancy is not so important in subcritical regions which are far enough from critical points and where the gas and liquid states are well separated in density. However, with approaching critical points, the relative level of thermodynamic inconsistency becomes too high, resulting in no solution to the EPCP equations (Eq. (25)). Because of this, an alternative Maxwell construction (MWC) scheme has also been utilized. It can be derived by integrating the above Gibbs-Duhem relation and substituting

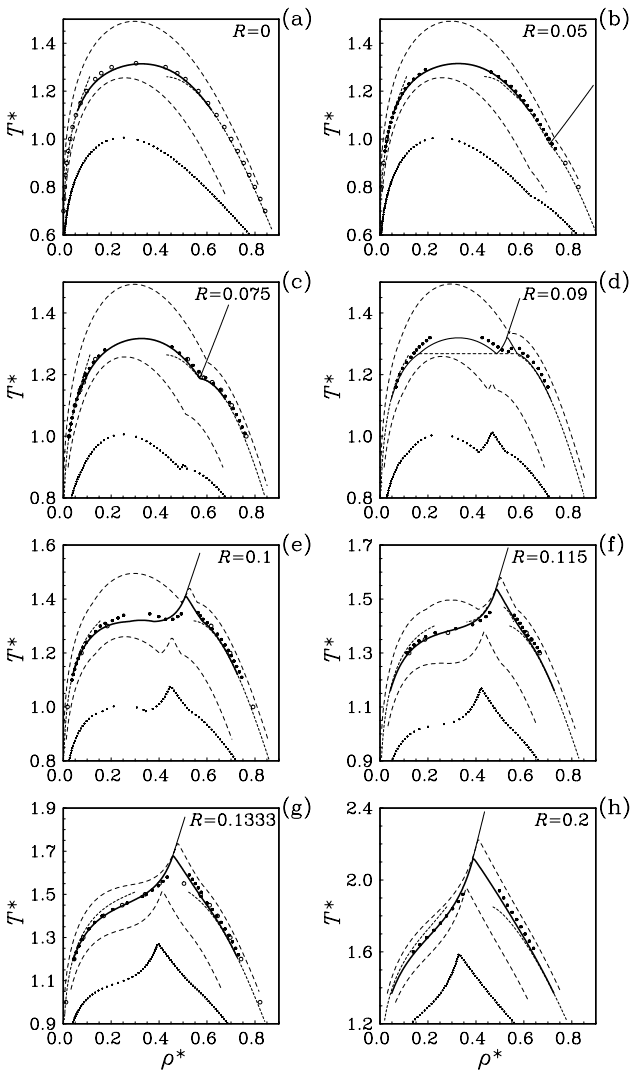

Fig. 1. The gas-liquid and liquid-liquid binodals of the LJ-YK Ising fluid obtained for different ratios R within the OZ-DH-FC approach at $B = 0$ using the EPCP (short-dashed curves) and MWC (solid curves) schemes. The OZ-SMSA-FC and OZ-KH-FC results are given by the upper and lower lying dashed curves, respectively. The GEMC and MHR data are shown as open and full circles, respectively. The MF predictions are presented by the dotted curves. The triple point is represented as the horizontal dashed line. The magnetic transition is plotted by the thin lines.

the obtained chemical potential into the second line of equation (25). Then one finds,

$$P\big(\rho^{\mathrm{I}},T,B\big) = P\big(\rho^{\mathrm{II}},T,B\big) = \mathcal{P}\,,$$
$$\left(\frac{1}{\rho^{\mathrm{I}}} - \frac{1}{\rho^{\mathrm{II}}}\right)\mathcal{P} = \int_{\rho^{\mathrm{I}}}^{\rho^{\mathrm{II}}} P(\rho,T,B)\,\frac{\mathrm{d}\rho}{\rho^2}\,, \tag{27}$$

where $\mathcal{P}$ denotes the coexistence pressure.

It is worth mentioning that contrary to the EPCP approach, the MWC scheme requires the existence of continuous (van der Waals-like) isotherms $P(\rho,T,B)$ inside

the whole two-phase region $\rho \in [\rho^{\rm I}, \rho^{\rm II}]$ (to perform the integration according to Eq. (27)). At the same time, the computations show that the original OZ-DH-FC solutions to the correlation functions disappear when approaching a metastable ($\partial P(\rho, T, B)/\partial\rho|_{T,B} < 0$) region which lies inside the $[\rho^{\rm I}, \rho^{\rm II}]$-density interval. Other IE approaches may lead to the existence of solutions even in the metastable region. A typical example is the OZ-SMSA-FC approach for Ising fluids with YK magnetic and YK attractive nonmagnetic interactions [21]. In order to ensure that this is also the case for the LJ-YK Ising fluid model, the SMSA bridge function $b_{\alpha\beta}(r) = \ln[1 + s_{\alpha\beta}(r)] - s_{\alpha\beta}(r)$ complimented by the standard WCA partitioning $\varphi_{\rm lr}(r) = \varphi(r) - \varphi_{\rm s}(r)$ of the LJ part [45] of the total potential (Eq. (9)) has also been considered (see the definition of $\varphi_{\rm s}(r)$ just after Eq. (11)). Another important example is the Kovalenko and Hirata (KH) closure [60,61] which has the form $b_{\alpha\beta}(r) = \ln[1 + \tau_{\alpha\beta}(r)] - \tau_{\alpha\beta}(r)$ for $\tau_{\alpha\beta} = h_{\alpha\beta} - c_{\alpha\beta} > 0$ and $b_{\alpha\beta}(r) = 0$ at $\tau_{\alpha\beta} \leq 0$. The KH approach combines in fact the SMSA and HNC bridge functions and does not require any partitioning. Being applied to the LJ-Yukawa Ising fluids, the corresponding KH version will be referred to as the OZ-KH-FC one.

Despite the fact that in the metastable regions there are no solutions to the original OZ-DH-FC integral equations (see above), our investigations show that such solutions nevertheless can be obtained by reducing the r-domain size to relatively small values $r_{\max} \sim 5\sigma$. This reduction can be considered as a modification of the original DH-like partitioning scheme (Eqs. (10) and (11)), where the latter corresponds to the limiting case $r_{\max} \to \infty$. The finite-size effects have been taken into account by adding the appropriate corrections (like in MC simulations) to the virial pressure P (and $\mu_{+,-}$). In particular, the pressure has been corrected by performing analytically the integration in Eq. (20) over r in the interval $[r_{\max}, \infty]$ assuming $g_{\alpha\beta}(r) = 1$ for $r > r_{\max}$. The DH modification allows us to reproduce a continuous shape of the binodals in the critical regions. A more rigorous description requires the enforcing of the thermodynamic self-consistency between different (virial, energy, and compressibility) routes. This question presents a very difficult problem which up to date is not completely solved even for pure LJ systems. It goes beyond the scope of the current study of more complicated Ising fluids and can be the subject of further investigations.

The MWC results obtained within the modified OZ-DH-FC scheme at $r_{\max} = 5\sigma$ are presented in Figure 1 by the solid curves. They appear to be very close to the EPCP predictions in the subcritical regions. When approaching critical points, the increased discrepancy between the EPCP and MWC binodals indicates an increased relative level of thermodynamic inconsistency of the original DH approximation. The computations have shown that in the subcritical regions the MWC results are virtually independent of the value of the truncation radius provided $r_{\max} \geq 5\sigma$, so that the finite-size effects have indeed been taken into account properly. Moreover, the MWC binodals practically coincide with MC simulation data in a wide temperature and density range. The results corresponding to the OZ-SMSA-FC approach (within the MWC scheme) and the OZ-KH-FC description are also included in Figure 1. In these cases, the agreement with the simulation data is significantly worse than within the OZ-DH-FC description. In particular, like for the pure LJ system (subset (a) of Fig. 1), the OZ-SMSA-FC theory overestimates while the OZ-KH-FC description underestimates considerably the critical temperatures of the LJ-YK Ising fluid for any ratio $R \geq 0$ (see subsets (b)–(h)). It is worth emphasizing that the KH description is thermodynamically self-consistent between the virial and energy routes [60] (but not with the compressibility one) and thus satisfies exactly the Gibbs-Duhem relation. For this reason, both MWC and EPCP versions of the OZ-KH-FC theory will lead to identical results. Note also that the OZ-SMSA-FC results correspond to the SMSA bridge function with the WCA partitioning of the LJ part of the total potential, while the OZ-DH-FC description deals with the DH bridge function and the DH partitioning scheme. The hybrid scheme with the SMSA bridge function complimented by the DH partitioning improves the results with respect to the original SMSA-WCA ansatz, but they are worse (and not shown in Fig. 1) than the OZ-DH-FC ones. On the other hand, the hybridization of the DH closure with the WCA partitioning leads to worse results (they shift to the SMSA-WCA ones and are not shown in Fig. 1) with respect to those of the original OZ-DH-FC description. We see therefore, that the IE results are sensitive to both the form of the approximate bridge function and the way of partitioning the potential (in the hypothetical case of the exact closure the results should be independent of the partitioning).

3.2.2 MF versions

In the original MF work [19], the van der Waals-like (vdW) equation of state $P(\rho, T, B) = P_{\rm s} - \rho^2(a_\varepsilon + a_\epsilon m^2)/2$ with the excluded volume approximation $P_{\rm ev} = \rho k_{\rm B}T/(1 - \rho v)$ for the reference pressure $P_{\rm s}$ and the mean field magnetization $m = \tanh[(B + a_\epsilon \rho m)/(k_{\rm B}T)]$ has been used. The ratio of magnetic to the attractive part of nonmagnetic interactions has been introduced as $R_{\rm MF} = a_\epsilon/a_\varepsilon$. However, no explicit relations connecting the macroscopic parameters v, a_ϵ and a_ε with the parameters of the LJ-YK potentials (Eqs. (2) and (3)) have been, in fact, presented. This leads to difficulties of direct comparison between the OZ-DH-FC and MF results since the correspondence between the LJ-YK ratio R (Eq. (26)) and $R_{\rm MF}$ remains unknown. Moreover, in 3D fluids it is more natural to deal with the Carnahan-Starling (CS) expression [62] $P_{\rm s} = \rho k_{\rm B}T(1 + \eta + \eta^2 - \eta^3)/(1 - \eta)^3$ for the reference pressure, where $\eta = \rho v/4$ denotes the packing fraction, rather than with the vdW excluded volume one. The CS pressure is quasiexact for 3D hard sphere systems and coincides with the vdW counterpart only in the low density regime ($\rho^* \ll 1$) where both expressions have the same asymptotics, $P_{\rm ev}|_{\rho^* \ll 1} = \rho k_{\rm B}T(1 + \rho v + \mathcal{O}(\rho^2))$ and

$P_{\rm s}|_{\rho^*\ll 1} = \rho k_{\rm B}T(1+4\eta+\mathcal{O}(\eta^2)) = \rho k_{\rm B}T(1+\rho v+\mathcal{O}(\rho^2))$ (the higher-order terms $\mathcal{O}(\rho^2)$ have been neglected).

The required correspondence can be derived by extending our recent MF development [20] for ideal Ising fluids to the nonideal LJ-YK Ising case. Acting in the spirit of reference [20], one finds that the macroscopic parameters a_ε and a_ϵ should be related to the LJ and YK potentials as $a_\varepsilon = -4\pi\int_0^\infty g_{\rm s}(r)\varphi_{\rm a}(r)r^2{\rm d}r$ and $a_\epsilon = 4\pi\int_0^\infty g_{\rm s}(r)J(r)r^2{\rm d}r$, where $g_{\rm s}(r)$ denotes the radial distribution function of the reference system with the repulsion part $\varphi_{\rm s}(r)$ of the LJ potential and $\varphi_{\rm a}(r) = \varphi(r) - \varphi_{\rm s}(r)$ represents the LJ attractive part. Since the van der Waals description is itself only approximate, the quantities a_ε, a_ϵ and v can be approximated as well within the same order of accuracy. One of the ways lies in the representation of the reference system by a system of hard spheres with some effective diameter $\sigma_{\rm s}$. The latter can be determined by requiring the second virial coefficients related to the hard sphere system with the particle diameter $\sigma_{\rm s}$ and the reference system with the repulsion potential $\varphi_{\rm s}$ to be equal. This leads [20] to the value $\sigma_{\rm s}^3(T) = 3\int_0^\infty(1-\exp[-\varphi_{\rm s}(r)/(k_{\rm B}T)])r^2{\rm d}r$, so that the excluded volume per particle and the packing fraction of the hard sphere system are equal to $v = 2\pi\sigma_{\rm s}^3/3$ and $\eta = \rho v/4 = \pi\rho\sigma_{\rm s}^3/6$, respectively. Further, the radial distribution function of the reference system can be approximated by that of the hard sphere system in the low density regime, $g_{\rm s}(r) \approx \Theta(r-\sigma_{\rm s})$, where Θ denotes the unit Heaviside function, i.e., $\Theta(r-\sigma_{\rm s}) = 1$ for $r \geq \sigma_{\rm s}$ and $\Theta(r-\sigma_{\rm s}) = 0$ for $r < \sigma_{\rm s}$. This allows to perform the analytical integration $a_\varepsilon \approx -4\pi\int_{\sigma_{\rm s}}^\infty \varphi_{\rm a}(r)r^2{\rm d}r = 4\pi\varepsilon(8\sqrt{2}\sigma^3 - 3\sigma_{\rm s}^3)/9$ (at $\sigma_{\rm s} \leq 2^{1/6}\sigma$) and $a_\epsilon \approx 4\pi\int_{\sigma_{\rm s}}^\infty J(r)r^2{\rm d}r = 4\pi\epsilon\sigma^2(\sigma+\sigma_{\rm s}){\rm e}^{1-\sigma_{\rm s}/\sigma}$. Computations show that the effective diameter $\sigma_{\rm s}$ appears to be very close to the LJ size σ of the particles for characteristic temperatures of order $T^* \sim 1$. For instance, $\sigma_{\rm s}$ varies from 1.03σ to 0.99σ with varying the temperature in a typical interval of $T^* \in [0.6, 2]$. In such a case, we can put $\sigma_{\rm s} \approx \sigma$ without loss of precision and obtain $a_\varepsilon \approx 4\pi\varepsilon\sigma^3(8\sqrt{2}-3)/9$ and $a_\epsilon \approx 8\pi\epsilon\sigma^3$. This immediately yields $R_{\rm MF} = a_\epsilon/a_\varepsilon = 18R/(8\sqrt{2}-3) \approx 2.165R$, i.e., the MF ratio should be nearly two times larger with respect to R.

Our MF calculations have been performed using the vdW-like equation of state $P(\rho,T,B) = P_{\rm s} - \rho^2(a_\varepsilon + a_\epsilon m^2)/2$ with the CS reference pressure $P_{\rm s}$ at $\eta = \pi\rho\sigma^3/6 = \pi\rho^*/6$ (this version will be referred to as MFvdWCS). The results of these calculations are given in Figure 1 as well. The MF binodals have been plotted for the ratios $R_{\rm MF} = 0$, 0.1082, 0.1624, 0.1948, 0.2165, 0.249, 0.2887, and 0.433 in subsets (a)–(h) respectively, to satisfy the above requirement $R_{\rm MF} = 2.165R$. It can be seen that the deviations in this case from the MC simulation data and OZ-DH-FC results are more significant than for the OZ-SMSA-FC and OZ-KH-FC approaches. In particular, the critical temperature and density are so underestimated that the discrepancy appears to be much larger than that of any version of the IE theory considered. As was expected, the MF approach can lead only to a qualitative description of the phase diagram behavior.

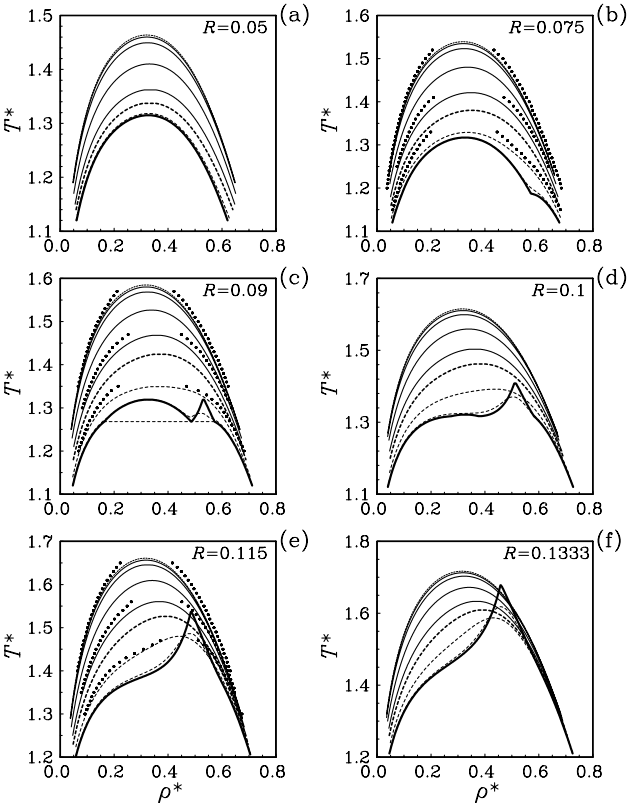

Fig. 2. The OZ-DH-FC phase diagrams of the LJ-YK Ising fluid for typical values of R and $B^* = 0$ (bold solid curves), 0.01 (thin dashed), 0.1 (dashed), 0.3 (bold dashed), and (bottom to top, solid) $B^* = 0.5$, 1, 2, 3, and $B^* = \infty$ (dotted). The MHR data (circles) are shown for $B^* = 0.1$, 0.5, and 2. The triple point is plotted by the horizontal dashed line.

3.3 Nonzero magnetic field

The OZ-DH-FC phase diagrams of the LJ-YK Ising fluid obtained in the presence of an external magnetic field within the MWC scheme are plotted in Figure 2 for typical values of B and R. For the purpose of comparison, MHR examples are also included. On the basis of the results shown in Figures 1 and 2 we can point out four types of the phase diagram topology overall. For $R_{\rm u} = 0.1 < R < \infty$ (type I), the system exhibits a tricritical point (TCP) behavior at $B = 0$, see subsets (e)–(h) of Figure 1 and (d)–(f) of Figure 2. This is similar to the ideal Ising fluid with a soft-core repulsion potential [20,21]. With turning on the external field ($B \neq 0$), the TCP transforms into a gas-liquid critical point (GLCP). For $R_{\rm l} = 0.075 < R < 0.1 = R_{\rm u}$ (type II), beside the TCP, a GLCP exists even at $B = 0$ in the paramagnetic phase region, see subset (d) of Figure 1 and (c) of Figure 2. The TCP now corresponds to a liquid-liquid transition between the paramagnetic and ferromagnetic phases. Here, a triple point occurs too, where a rarefied paramagnetic gas, a dense paramagnetic liquid, and a highly dense ferromagnetic liquid coexist at the same temperature T and pressure P (horizontal dashed lines in Figs. 1d and 2c). In the presence of the external field, region II splits

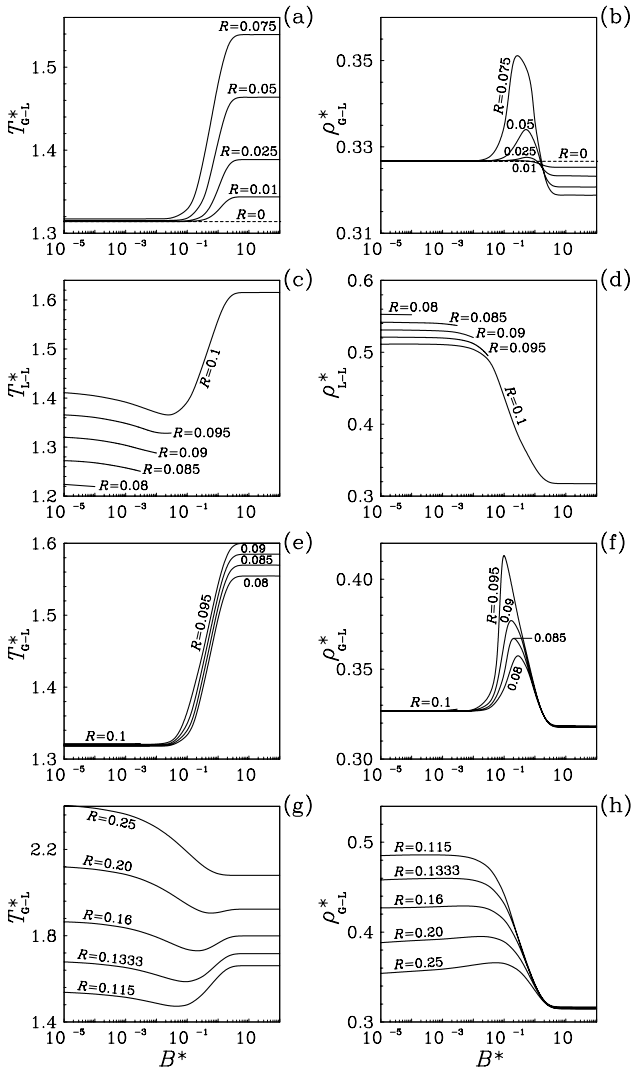

Fig. 3. The critical temperatures and critical densities of gas-liquid and liquid–liquid phase transitions in the LJ-YK Ising fluid as functions of external field B at different R.

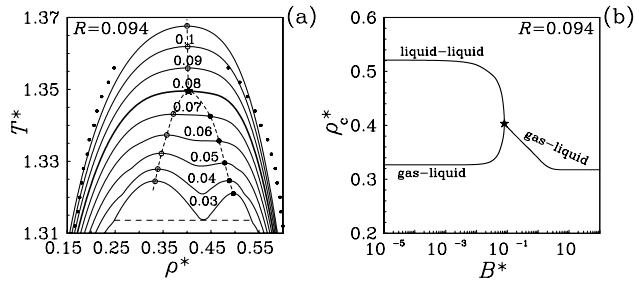

Fig. 4. The same as in Figures 2 and 3 but at a specific van Laar value of $R = R_{\rm vL}$. The asymmetric tricritical point is shown by a star. The binodals are plotted in subset (a) for different B^* varying from 0.03 (bottom) to 0.11 (top). The MHR data (circles) are shown in (a) for $B^* = 0.09$.

into two subregions in dependence of whether the gas-liquid (type IIa, $R_{\rm vL} < R < R_{\rm u}$) or liquid-liquid (type IIb, $R_{\rm l} < R < R_{\rm vL}$) critical line terminates at some finite value $B \neq 0$, where $R_{\rm vL} = 0.094$. If $R \leq R_{\rm l} = 0.075$ (type III), the spatial interaction dominates over the spin one, so that the GLCP remains, while the TCP transforms into a critical end point (CEP), see subsets (b) and (c) of Figure 1. At $B \neq 0$, the CEP disappears, while the influence of the external field on the GLCP becomes weaker and weaker with decreasing R (see subsets (a) and (b) of Fig. 2). At $R = 0$ we come to the pure LJ fluid with the existence of only the GLCP (see subset (a) of Fig. 1).

The gas-liquid and liquid-liquid critical temperatures $T^*_{\rm G-L}$ and $T^*_{\rm L-L}$ as well as the critical densities $\rho^*_{\rm G-L}$ and $\rho^*_{\rm L-L}$ are shown in Figure 3 as functions of the external field strength B^*. It is obvious that for $R = 0$ the results are independent of B. At small R, the modifications of the phase diagrams with increasing B are monotonic in $T_{\rm G-L}$, but they are nonmonotonic in the gas-liquid critical density $\rho^*_{\rm G-L}$ (see subsets (a) and (b) of Figs. 2 and 3). At intermediate R, the functions $T_{\rm G-L}(B)$ and $\rho_{\rm G-L}(B)$ behave similarly (subsets (e) and (f) of Fig. 3) as for small R. On the other hand, the liquid-liquid functions $T_{\rm L-L}(B)$ and $\rho_{\rm L-L}(B)$ behave quite differently, namely, the critical temperature starts to behave nonmonotonically, while the critical density monotonically decreases (subsets (c) and (d) of Figs. 2 and 3). For larger R, the function $T_{\rm G-L}(B)$ is nonmonotonic with the existence of a minimum. With further increasing $R \geq 0.25$ it becomes monotonically decreasing with rising B (subset (g) of Fig. 3). At the same time, in the ideal-like regime $R \geq 0.25$, the critical density $\rho_{\rm G-L}(B)$ behaves nonmonotonically with the presence of a maximum at some finite B (subset (h) of Fig. 3). Such a complicated behavior is explained by a subtle interplay between the translational and spin degrees of freedom. In the infinite external field limit $B \to \infty$ all the spins take the same value $s = +1$. Then the Ising spin system transforms into a simple nonmagnetic LJ-YK fluid with the interparticle potential $\phi(r) \to \varphi(r) - J(r)$ (see Eq. (1)) and the existence of only the gas-liquid critical point for arbitrary values of R (see Figs. 2 and 3).

Under special conditions, namely, at the boundary value $R_{\rm vL} = 0.094$, an unsymmetrical tricritical (so-called van Laar) point arises additionally. The corresponding phase diagrams and dependencies of the critical lines on the external field strength are presented in subsets (a) and (b) of Figure 4. The gas-liquid (on the left in subset (a) and on the bottom in subset (b)) and liquid-liquid (on the right in subset (a) and on the top in subset (b)) critical points are shown in subset (a) as open and full squares, respectively, connected by dashed curves, and as lower and upper lying solid curves in subset (b). The curves meet in the unsymmetrical tricritical point (star). It is identified at $B^*_{\rm vL} \approx 0.08$, $T^*_{\rm vL} \approx 1.35$, and $\rho^*_{\rm vL} \approx 0.40$.

Phase diagrams similar to those found for the LJ-YK Ising fluid are observed for other systems, such as YK-YK Ising [21], XY [22,23], and Heisenberg [7,12] spin fluid models, symmetric binary nonmagnetic mixtures [29–36], mixtures of ^{3}He-^{4}He [39–41], Stockmayer fluids [63], etc. The van Laar point was previously identified in the YK-YK Ising [21] and XY [22,23] spin fluids as well as in symmetric mixtures [64]. Different spin fluid models differ in

Table 1. Boundary ratios of magnetic to nonmagnetic interactions corresponding to different Ising fluid models (see text for notation).

Model	$R_{\rm l}$	$R_{\rm vL}$	$R_{\rm u}$	References
LJ-YK	0.075	0.094	0.100	this work
YK-YK	0.140	0.196	0.215	[21]
MFvdWCS	0.149	0.209	0.231	this work
MFvdW	0.211	0.279	0.304	[2,64]

their critical temperature and density dependencies on the external field B. For example, in the ideal regime, when R is large enough to neglect the influence of attractive nonmagnetic interactions, the gas-liquid critical temperature decreases monotonically with increasing B for the Ising model, while it behaves nonmonotonically for the XY and Heisenberg systems [20–23,26]. For our case of the LJ-YK Ising model, the ideal regime is observed for $R \geq 0.25$ (see subset (g) of Fig. 3). The pattern complicates significantly in the nonideal regime, when both magnetic and nonmagnetic interactions should be taken into account. Here, the critical temperature and critical density depend on the strength of the external field in a very complicated way with various possible scenarios in dependence on the value of R (see subsets (a)–(h) in Fig. 3).

3.4 Boundary relations

The differences in the phase diagram behavior of YK-YK and LJ-YK spin fluids appear in their different lower ($R_{\rm l}$), upper ($R_{\rm u}$) and van Laar ($R_{\rm vL}$) boundary ratio values at which the diagrams change their topology. The IE boundary values found in this work for the LJ-YK Ising fluid model are collected in Table 1. For the purpose of comparison, the IE results for the YK-YK Ising model [21] are included as well. In the latter case, the ratio of magnetic to nonmagnetic interactions was introduced as $R_{\rm YK} = \epsilon/\epsilon_I > 0$, where ϵ_I denotes the intensity of the YK nonmagnetic attractive (sign "−") potential $I(r) = -\epsilon_I\sigma\exp[-(r-\sigma)/\sigma]/r$ (cf. Eq. (3)). The MF boundary values obtained in this work for the vdWCS Ising model (see Sect. 3.2.2) are labeled as MFvdWCS and presented in the table too (here $R_{\rm l}$ and $R_{\rm u}$ were calculated numerically, while $R_{\rm vL}$ was interpolated). The previously known MF results for the vdW Ising fluid [2,64], marked by MFvdW, are also shown. Note that, in fact, $R_{\rm l}$ and $R_{\rm u}$ were obtained in reference [2] for the 1D Ising fluid (where the excluded volume pressure transforms into Tonk's counterpart), while $R_{\rm vL}$ was evaluated in reference [64] for a symmetric binary mixture. These MF results demonstrate the obvious change of the boundary values when turning from the excluded volume approximation to the quasiexact CS reference pressure.

A simple approximate relation between the YK-YK and LJ-YK boundary values can be found by introducing a generalized ratio $\mathcal{R}$ of integrated strengths (as defined by Eq. (25) of Ref. [21]) and assuming that different Ising models with the same value of $\mathcal{R}$ should belong to the same phase diagram topology. Then for the YK-YK model one finds $\mathcal{R} = -\int g(r)J(r){\rm d}\mathbf{r}/\int g(r)I(r){\rm d}\mathbf{r} \equiv R_{\rm YK}$, where $g(r) = x^2 g_{++}(r) + 2x(1-x)g_{+-}(r) + (1-x)^2 g_{--}(r)$ is the total radial distribution function of the Ising fluid. Thus $R_{\rm YK}$ simply reduces to $\mathcal{R}$ independently of $g(r)$, because the functions $J(r)$ and $I(r)$ are of the same YK form. For the LJ-YK model, the ratio $\mathcal{R} = -\int g(r)J(r){\rm d}\mathbf{r}/\int g(r)\varphi(r){\rm d}\mathbf{r} > 0$ cannot be evaluated analytically since the functions $J(r)$ and $\varphi(r)$ are of the qualitatively different YK and LJ forms (sign "−" arises because J and φ enter in the Hamiltonian under different signs, see Eq. (1)) and the result will depend on $g(r)$. The radial distribution in the Ising fluid is a complicated function of the interparticle distance r, density ρ, magnetization $m = 2x - 1$, temperature T, and parameter R. To simplify calculations, it can be approximated by its functional form in the low density and magnetization ($x \sim 1/2$) regime, i.e., $g(r) \approx (\mathrm{e}^{-(\varphi(r)+J(r))/(k_{\rm B}T)} + \mathrm{e}^{-(\varphi(r)-J(r))/(k_{\rm B}T)})/2$. For a typical temperature of order $T^* \sim T^*_{\rm vL} \approx 1.35$ and $R \sim 0.1$ this yields $\mathcal{R} = -\int g(r)J(r){\rm d}\mathbf{r}/\int g(r)\varphi(r){\rm d}\mathbf{r} \approx 1.92R$ (factor $\mathcal{R}$ almost does not change with varying T and other parameters in the region investigated), and thus $R_{\rm YK}/R \approx 1.92$. At the same time, as was derived in Section 3.2.2, the MFvdWCS and LJ-YK ratios should be connected by the relation $R_{\rm MF}/R \approx 2.17$, so that $R_{\rm MF}/R_{\rm YK} \approx 2.17/1.92 \approx 1.13$. The ratios of boundary values $R_{\rm l,u,vL}$ corresponding to MFvdWCS and YK-YK, MFvdWCS and LJ-YK as well as YK-YK and LJ-YK models are shown in Table 2 (marked by $D_{\rm l,u,vL}$) together with the above predictions (labeled as D). In practice, these predictions will be satisfied of course only approximately, reflecting the level of precision of the simplified assumptions made during their derivations. As can be seen, the actual ratios $D_{\rm l,u,vL}$ are not constant and slightly increase with increasing R, but the deviations from D in each of the cases are small. In such a way, the boundary ratios related to different Ising spin fluid models can be nearly mapped one onto another calculating only one generalized $\mathcal{R}$ coefficient.

Table 2. Relations between boundary ratios of different Ising fluid models (see text for notation).

Model	$D_{\rm l}$	$D_{\rm vL}$	$D_{\rm u}$	D
MFvdWCS/YK-YK	1.06	1.07	1.07	1.13
MFvdWCS/LJ-YK	1.99	2.22	2.31	2.17
YK-YK/LJ-YK	1.87	2.09	2.15	1.92

4 Conclusion

We have proposed an IE extension of the DH approach to fluids with both LJ translational and YK Ising spin interactions in the presence of an external magnetic field. It combines the standard OZ method with a specific Duh-like partitioning of the total potential. A comparison with simulations for the LJ-YK Ising spin fluid has shown that the theory is efficient to provide a quantitative calculation of the complicated phase diagrams in subcritical and critical regions. It can be extended to systems with XY and

Heisenberg spin degrees of freedom or with dipole interactions. These problems as well as the improvement of the thermodynamic self-consistency of the IE approach can be considered in further studies.

This work was supported in part by the Fonds zur Förderung der wissenschaftlichen Forschung under Project No. 18592-PHY. I.O. and I.M. thank the Fundamental Researches State Fund of the Ministry of Education and Science of Ukraine for support under Project No. 02.07/00303.

References

1. N.E. Frankel, C.J. Thompson, J. Phys. C: Solid State Phys. **8**, 3194 (1975)
2. P.C. Hemmer, D. Imbro, Phys. Rev. A **16**, 380 (1977)
3. E. Lomba, J.J. Weis, N.G. Almarza, F. Bresme, G. Stell, Phys. Rev. E **49**, 5169 (1994)
4. J.M. Tavares, M.M. Telo da Gama, P.I.C. Teixeira, J.J. Weis, M.J.P. Nijmeijer, Phys. Rev. E **52**, 1915 (1995)
5. M.J.P. Nijmeijer, J.J. Weis, Phys. Rev. E **53**, 591 (1996)
6. M.J.P. Nijmeijer, J.J. Weis, in *Annual Review of Computational Physics IV*, edited by D. Stauffer (World Scientific, Singapore, 1996)
7. J.J. Weis, M.J.P. Nijmeijer, J.M. Tavares, M.M. Telo da Gama, Phys. Rev. E **55**, 436 (1997)
8. M.J.P. Nijmeijer, A. Parola, L. Reatto, Phys. Rev. E **57**, 465 (1998)
9. F. Lado, E. Lomba, Phys. Rev. Lett. **80**, 3535 (1998)
10. T.G. Sokolovska, Physica A **253**, 459 (1998)
11. F. Lado, E. Lomba, J.J. Weis, Phys. Rev. E **58**, 3478 (1998)
12. F. Schinagl, H. Iro, R. Folk, Eur. Phys. J. B **8**, 113 (1999)
13. F. Schinagl, R. Folk, H. Iro, Condens. Matter Phys. **2**, 313 (1999)
14. T.G. Sokolovska, R.O. Sokolovskii, Phys. Rev. E **59**, R3819 (1999)
15. T.G. Sokolovska, R.O. Sokolovskii, M.F. Holovko, Phys. Rev. E **62**, 6771 (2000)
16. E. Lomba, F. Lado, J.J. Weis, Condens. Matter Phys. **4**, 45 (2001)
17. I.M. Mryglod, I.P. Omelyan, R. Folk, Phys. Rev. Lett. **86**, 3156 (2001)
18. W. Fenz, R. Folk, Phys. Rev. E **67**, 021507 (2003)
19. W. Fenz, R. Folk, Condens. Matter Phys. **6**, 675 (2003)
20. W. Fenz, R. Folk, I.M. Mryglod, I.P. Omelyan, Phys. Rev. E **68**, 061510 (2003)
21. I.P. Omelyan, I.M. Mryglod, R. Folk, W. Fenz, Phys. Rev. E **69**, 061506 (2004); **70**, 049903(E) (2004)
22. I.P. Omelyan, W. Fenz, I.M. Mryglod, R. Folk, Phys. Rev. Lett. **94**, 045701 (2005)
23. I.P. Omelyan, W. Fenz, I.M. Mryglod, R. Folk, Phys. Rev. E **72**, 031506 (2005)
24. W. Fenz, I.P. Omelyan, R. Folk, Phys. Rev. E **72**, 056121 (2005)
25. W. Fenz, R. Folk, Phys. Rev. E **71**, 046104 (2005)
26. R.O. Sokolovskii, Phys. Rev. B **61**, 36 (2000)
27. S. Romano, R.O. Sokolovskii, Phys. Rev. B **61**, 11379 (2000)
28. E. Lomba, M. Alvarez, L.L. Lee, N.G. Almarza, J. Chem. Phys. **104**, 4180 (1996)
29. N.B. Wilding, F. Schmid, P. Nielaba, Phys. Rev. E **58**, 2201 (1998)
30. G. Kahl, E. Schöll-Paschinger, A. Lang, Monatshefte für Chemie **132**, 1413 (2001)
31. E. Schöll-Paschinger, D. Levesque, J.J. Weis, G. Kahl, Phys. Rev. E **64**, 011502 (2001)
32. G. Kahl, E. Schöll-Paschinger, G. Stell, J. Phys.: Condens. Matter **14**, 9153 (2002)
33. O. Antonevych, F. Forstmann, E. Diaz-Herrera, Phys. Rev. E **65**, 061504 (2002)
34. E. Schöll-Paschinger, G. Kahl, J. Chem. Phys. **118**, 7414 (2003)
35. D. Pini, M. Tau, A. Parola, L. Reatto, Phys. Rev. E **67**, 046116 (2003)
36. N.B. Wilding, Phys. Rev. E **67**, 052503 (2003)
37. E. Schöll-Paschinger, G. Kahl, J. Chem. Phys. **123**, 134508 (2005)
38. G. Pastore, R. Santin, S. Taraphder, F. Colonna, J. Chem. Phys. **122**, 181104 (2005)
39. M. Blume, V.J. Emery, R.B. Griffiths, Phys. Rev. A **4**, 1071 (1971)
40. A. Maciolek, M. Krech, S. Dietrich, Phys. Rev. E **69**, 036117 (2004)
41. D.J. Tulimieri, J. Yoon, M.H.W. Chan, Phys. Rev. Lett. **82**, 121 (1999)
42. B. Kraft, H. Alexander, Phys. Konden. Mater. **16**, 281 (1973)
43. T. Albrecht, C. Bührer, M. Fähnle, K. Maier, D. Platzek, J. Reske, Appl. Phys. A **65**, 215 (1997)
44. J.D. Weeks, D. Chandler, H.C. Andersen, J. Chem. Phys. **54**, 5237 (1971)
45. N. Choudhury, S.K. Ghosh, J. Chem. Phys. **116**, 8517 (2002)
46. F. Lado, S.M. Foiles, N.W. Ashcroft, Phys. Rev. A **28**, 2374 (1983)
47. G. Zerah, J.P. Hansen, J. Chem. Phys. **84**, 2336 (1985)
48. C. Caccamo, P.V. Giaquinta, G. Giunta, J. Phys.: Condens. Matter **5**, B75 (1993)
49. C. Caccamo, Phys. Rep. **274**, 1 (1996)
50. D.-M. Duh, A.D.J. Haymet, J. Chem. Phys. **103**, 2625 (1995)
51. D.-M. Duh, D. Henderson, J. Chem. Phys. **104**, 6742 (1996)
52. I. Omelyan, F. Hirata, A. Kovalenko, Phys. Chem. Chem. Phys. **7**, 4132 (2005)
53. J.P. Hansen, I.R. McDonald, *Theory of Simple Liquids*, 2nd edn. (Academic, London, 1986)
54. C.G. Gray, K.E. Gubbins, *Theory of Molecular Fluids*, Vol. 1 (Clarendon, Oxford, 1984)
55. J.G. Kirkwood, J. Chem. Phys. **3**, 300 (1935)
56. A. Kovalenko, S. Ten-no, F. Hirata, J. Comput. Chem. **20**, 928 (1999)
57. A.Z. Panagiotopoulos, Molec. Sim. **9**, 1 (1992)
58. A.M. Ferrenberg, R.H. Swendsen, Phys. Rev. Lett. **61**, 2635 (1988); **63**, 1195 (1989)
59. K. Binder, Rep. Prog. Phys. **60**, 487 (1997)
60. A. Kovalenko, F. Hirata, Chem. Phys. Lett. **349**, 496 (2001)
61. A. Kovalenko, F. Hirata, J. Chem. Phys. **110**, 10095 (1999)
62. N.F. Carnahan, K.E. Starling, J. Chem. Phys. **51**, 635 (1969)
63. B. Groh, S. Dietrich, Phys. Rev. Lett. **72**, 2422 (1994)
64. P.H. von Konynenburg, R.L. Scott, Philos. Trans. R. Soc. London A **298**, 495 (1980)